Journal of Power Sources 270 (2014) 569–575

Contents lists available at ScienceDirect

Journal of Power Sources

journal homepage: www.elsevier.com/locate/jpowsour

Variation of stress with charging rate due to strain-rate sensitivity of silicon electrodes of Li-ion batteries

Matt Pharr, Zhigang Suo, Joost J. Vlassak*

School of Engineering and Applied Sciences, Harvard University, Cambridge, MA 02138, USA

HIGHLIGHTS

- Increasing the charging rate results in an increase in stresses measured in a-Li_xSi.
- Observations indicate that rate-sensitive plasticity occurs in a-Li_xSi.
- A model of concurrent lithiation and rate-sensitive plasticity is developed.
- Rate-sensitive material parameters are quantified for a-Li_xSi.
- Results have important ramifications for rate-capabilities of silicon electrodes.

GRAPHICAL ABSTRACT

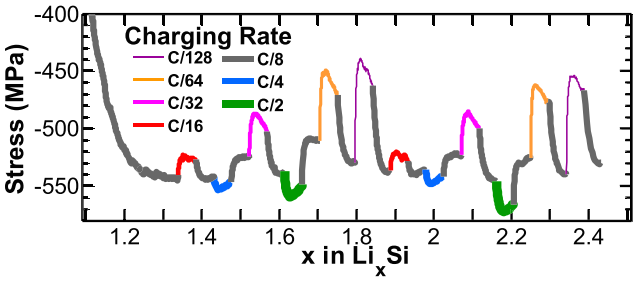

ARTICLE INFO

Article history:
Received 23 May 2014
Received in revised form
22 July 2014
Accepted 23 July 2014
Available online 1 August 2014

Keywords:
Lithium-ion batteries
Silicon
Plasticity
Fracture
Strain rate sensitivity
Creep

ABSTRACT

Silicon is a promising anode material for lithium-ion batteries due to its enormous theoretical energy density. Fracture during electrochemical cycling has limited the practical viability of silicon electrodes, but recent studies indicate that fracture can be prevented by taking advantage of lithiation-induced plasticity. In this paper, we provide experimental insight into the nature of plasticity in amorphous Li_xSi thin films. To do so, we vary the rate of lithiation of amorphous silicon thin films and simultaneously measure stresses. An increase in the rate of lithiation results in a corresponding increase in the flow stress. These observations indicate that rate-sensitive plasticity occurs in a-Li_xSi electrodes at room temperature and at charging rates typically used in lithium-ion batteries. Using a simple mechanical model, we extract material parameters from our experiments, finding a good fit to a power law relationship between the plastic strain rate and the stress. These observations provide insight into the unusual ability of a-Li_xSi to flow plastically, but fracture in a brittle manner. Moreover, the results have direct ramifications concerning the rate-capabilities of silicon electrodes: faster charging rates (i.e., strain rates) result in larger stresses and hence larger driving forces for fracture.

1. Introduction

Silicon has been identified as a promising anode material for lithium-ion batteries due to its ability to host a large amount of lithium [1]. Lithiation of silicon, however, causes an enormous volumetric expansion of ~300–400%, which under constraint can result in large mechanical stresses and fracture [2]. Fracture of the electrode leads to loss of active material and creates more surface area for solid-electrolyte interphase (SEI) growth, both of which significantly contribute to the fading of the capacity of the system [2-5]. Fortunately, this mechanical damage can be mitigated by nanostructuring the silicon anodes, as has been successfully demonstrated in nanowires [6,7], thin films [8–12], nanoporous structures [13,14], and hollow nanoparticles [15,16]. Specifically,

* Corresponding author. Tel.: +1 617 496 0424; fax: +1 617 495 9837.
E-mail address: vlassak@seas.harvard.edu (J.J. Vlassak).

http://dx.doi.org/10.1016/j.jpowsour.2014.07.153
0378-7753/

recent experiments and theories indicate that one can prevent fracture by taking advantage of lithiation-induced plasticity [11,17–22].

A number of studies have examined plastic deformation in Li_xSi [5,12,18,20–34]. Sethuraman et al. measured stresses during cycling of Li_xSi electrodes, finding plastic flow, which results in dissipation of energy comparable to that of polarization losses [18]. Zhao et al. suggested that plastic flow in a-Li_xSi reduces the energy release rate (i.e., the crack driving force), thus preventing fracture in nano-sized (~100 nm) electrodes [20]. Hertzberg et al. used nano-indentation to measure the hardness of nanocrystalline Li_xSi [23]. They found a linear variation of the hardness with the volume fraction of lithium, decreasing from 5 GPa for pure nanocrystalline silicon to 1.5 GPa for the fully lithiated phase ($Li_{15}Si_4$) [23]. Zhao et al. performed first-principles simulations of a-Li_xSi, attributing plastic flow to the continuous breaking and re-forming of Si–Si bonds [24]. Likewise, Fan et al. performed molecular dynamics simulations, finding lithiation-induced plastic softening due to the decreasing fraction of strong covalent Si–Si bonds and an increase in weak Li–Li bonds that facilitate plastic flow [25]. At large concentrations of lithium, they found that the high mobility of lithium facilitates bond breaking, switching, and re-forming in response to mechanical loading [25].

Beyond these studies, a number of questions remain concerning the nature of plasticity in Li_xSi. For instance, Pharr et al. measured the fracture energy of a-Li_xSi silicon thin films, finding that it demonstrates a peculiar ability to both flow plastically and fracture in a brittle manner [5]. The authors did not, however, speculate as to the physics governing this curious combination of properties. Brassart and Suo have suggested that inelasticity in high-capacity lithium-ion batteries may occur by two processes: flow and reaction [30]. The authors define "flow" as a process driven by deviatoric stress that preserves lithium concentration and volume, similar to plastic flow in a metal. By comparison, the authors define "reaction" as lithium insertion/removal: a process that changes the concentration and volume of the electrode [30]. One result of their theory is that lithium insertion (or removal) may enable flow at a lower stress than that needed for flow under pure mechanical loading. The applicability of this "reactive flow" theory to a-Li_xSi remains an open question. A study from first-principles calculations found the lithiation reaction to markedly reduce the flow stress of a-Li_xSi [27], while a molecular dynamics study found no such effects [25]. There are no experimental studies aimed at investigating these effects.

The purpose of this paper is to provide experimental insight into the nature of plasticity in a-Li_xSi. To do so, we vary the charging rate in amorphous silicon thin-film electrodes, while simultaneously measuring stresses that develop. The stresses are seen to increase monotonically with the charging rate. This observation cannot be explained by the "reactive-flow" effect, as has been suggested in literature [27,30]. Instead, these results indicate that rate-sensitive plasticity occurs at room temperature and at charging rates typical of lithium-ion batteries. These data are well described by a power law relationship between the plastic strain rate and the stress. These results also provide important insight into the unusual ability of a-Li_xSi to flow plastically, while fracturing in a brittle manner.

2. Experimental results

Using the substrate curvature technique, we measure stresses in thin-film electrodes of amorphous silicon during electrochemical testing. Details can be found in the Experimental procedure section. As a brief summary, 100 nm films of amorphous silicon on a glass substrate are lithiated and delithiated galvanostatically at a C/8 rate during the first cycle (8 h to fully lithiate and 8 more to fully delithiate). During the second cycle, the lithiation rate is varied systematically to investigate the effect of the charging rate on the stresses that develop in the electrode.

Fig. 1 shows a typical sequence of the applied charging rate and the response in the measured voltage. During the second lithiation, an increase in the charging rate results in a decrease in the voltage, as is normally observed in Li_xSi electrodes. We should note that the horizontal axis in the figure is constructed by integrating the current during the experiment to get the total charge. The amount of charge does not necessarily represent the concentration of lithium in silicon, as SEI formation may consume lithium during the first cycle. However, the main focus of this paper is related to the stress measurements as a function of charging rate (as shown in Fig. 2). These data are obtained during the second cycle, which minimizes the influence of the SEI on our measurements, as the majority of the SEI is formed during the initial lithiation [11].

Fig. 2 shows the stress measured in the film subject to the electrochemical cycling shown in Fig. 1. Fig. 2b is a zoomed-in view that focuses on the second lithiation. The legend shows the charging rate during each segment as expressed in the C-rate convention. Fig. 2b thus demonstrates that increasing the rate of lithiation results in a quick and sustained increase in the magnitude of the stress (the stress becomes more compressive). In fact, this increase in stress increases monotonically with charging rate – faster charging results in larger stress. We believe that these observations are indicative of a material rate-effect, i.e., plastic deformation of a-Li_xSi is rate sensitive, even at room temperature.

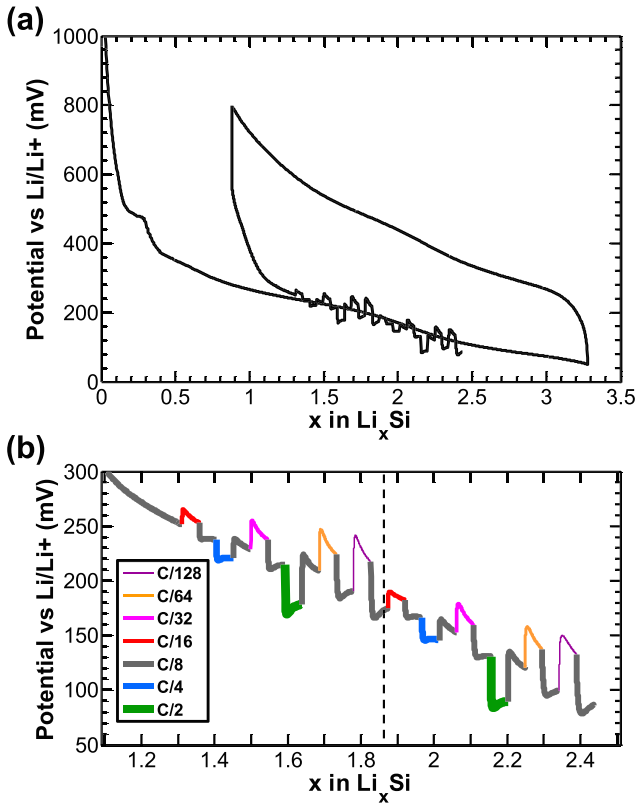

Fig. 1. Results of electrochemical cycling of a 100 nm Si thin-film electrode. (a) Measured potential as a function of lithium concentration. (b) A zoomed-in view that focuses on the second lithiation. The line thickness increases with the charging rate. The vertical dashed line indicates the point at which the set of charging rates is repeated.

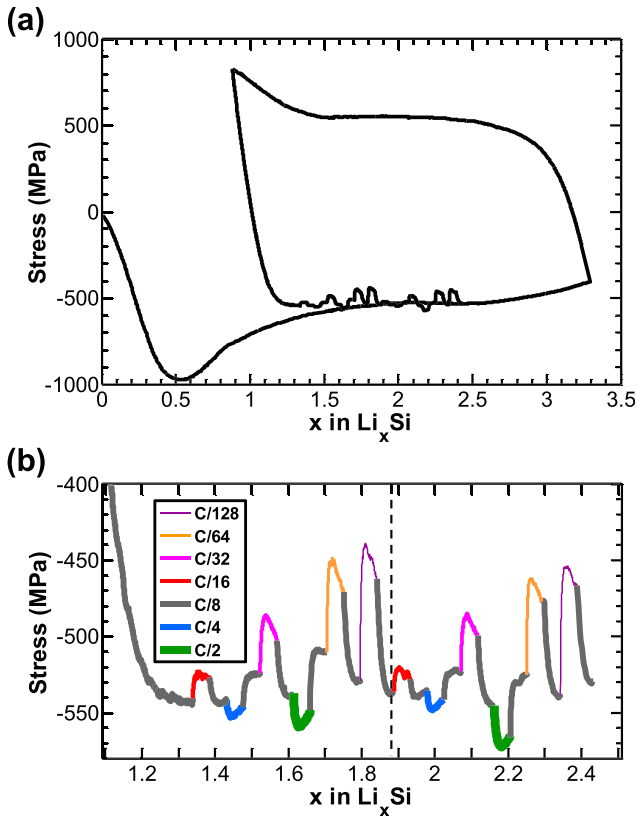

Fig. 2. (a) Stress measured in the 100 nm thin-film Si electrode subject to the electrochemical cycling conditions shown in Fig. 1. (b) A zoomed-in view that focuses on the second cycle. The line thickness increases with the charging rate. The vertical dashed line indicates the point at which the set of charging rates is repeated. A change in the charging rate results in a significant change in the stress.

3. A model of concurrent lithiation and rate-sensitive plasticity

We will now outline a simple mechanical model, with the goal of extracting material parameters from our experimental results. This model extends our previously developed models to account for rate-sensitive plasticity [5,20,21], and is similar to that developed by Bucci et al. [35]. Following these models [5,20,21,35], we take the deformation to consist of contributions from elasticity, plasticity, and lithiation-induced swelling. The total true strain, ε_{ij}, can then be written as.

$$\varepsilon_{ij} = \varepsilon_{ij}^{L} + \varepsilon_{ij}^{E} + \varepsilon_{ij}^{P}, \tag{1}$$

where ε_{ij}^{L} represents the true lithiation-induced strain, ε_{ij}^{E} represents the true elastic strain, and ε_{ij}^{P} represents the true plastic strain. For a thin film on a thick substrate, the state of stress is equi-biaxial, $\sigma_{11} = \sigma_{22} = \sigma$, with all other components of the stress vanishing. Due to the constraint of the substrate, the total in-plane components of the strain vanish, $\varepsilon_{11} = \varepsilon_{22} = \varepsilon = 0$. Eq. (1) becomes

$$\varepsilon^{L} + \varepsilon^{E} + \varepsilon^{P} = 0, \tag{2}$$

where the ε represent the in-plane components of the true strain. Note that while the total in-plane strain is zero, the individual strain terms associated elasticity, plasticity, and lithiation-induced swelling are not.

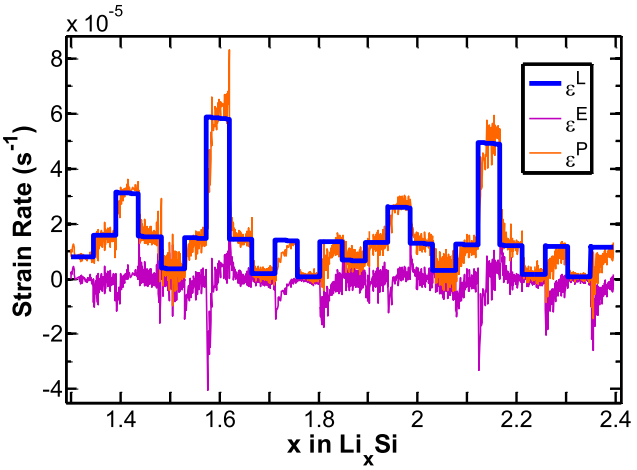

Fig. 3. Components of the strain rate in the 100 nm thin-film Si electrode subject to the electrochemical cycling conditions shown in Fig. 1. The thick blue line indicates the prescribed lithiation-induced strain rate, $\varepsilon^{L} = \beta/[3(1+\beta s)]\cdot ds/dt$. The thin purple line indicates the elastic component of the strain rate, $\varepsilon^{E} = (1-\nu_f)/E_f \cdot d\sigma/dt$. The thin orange line represents the plastic component of the strain rate, $\varepsilon^{P} = -1/\lambda^{P}\cdot d\lambda^{P}/dt$, as calculated from Eq. (7). (For interpretation of the references to colour in this figure legend, the reader is referred to the web version of this article.)

Following our previous work [5] and validated by experiments [5,36–38], we take the volume of the film, V_f, to be linear in the state of charge.

$$V_f = V_f^0(1+\beta s), \tag{3}$$

where V_f^0 is the initial volume of the film, β is related to the atomic volumes (Ω) by $\beta = (\Omega_{Li_{15}Si_4} - \Omega_{Si})/\Omega_{Si}$, and s is the state of charge, with a value of 0 representing pure silicon and a value of 1 representing the fully lithiated state (assumed to be a-$Li_{15}Si_4$ with a capacity of 3579 mAh g^{-1}) [36]. Obrovac et al. found a 280% increase in the volume of silicon upon reaching the fully lithiated state of $Li_{15}Si_4$ [36], i.e., $\beta = 2.8$. Using atomic force microscopy, He et al. and Beaulieu et al. measured similar values in patterned amorphous silicon films [37,38]. Both groups found that the volume increased linearly with lithium concentration [37,38].

Due to the amorphous nature of Li_xSi, the lithiation-induced deformation is assumed to be isotropic, such that the stretch ratios are equal, $\lambda_1^L = \lambda_2^L = \lambda_3^L = \lambda^L$. As in Ref. [5], we take $\lambda^L = (1+\beta s)^{1/3}$. By definition, the in-plane component of the true lithiation-induced strain is $\varepsilon^L = ln(\lambda^L)$, such that.

$$\varepsilon^{L} = \frac{1}{3}\ln(1+\beta s). \tag{4}$$

The elastic strains are given by Hooke's law.

$$\varepsilon^{E} = \frac{1-\nu_f}{E_f}\sigma, \tag{5}$$

where ν_f is Poisson's ratio of the film, E_f is the elastic modulus of the film, and σ is the in-plane component of the true (Cauchy) stress in the film.

The in-plane component of the true plastic strain will be left in a generalized form.

$$\varepsilon^{P} = \ln\left(\lambda^{P}\right). \tag{6}$$

Combining Eqs. (2) and (4–6), and taking a time-derivative, leads to.

$$-\frac{1}{\lambda^P}\frac{\mathrm{d}\lambda^P}{\mathrm{d}t}=\frac{\mathrm{d}}{\mathrm{d}t}\left[\frac{1-\nu_f}{E_f}\sigma\right]+\frac{\beta}{3(1+\beta s)}\frac{\mathrm{d}s}{\mathrm{d}t}. \tag{7}$$

In our experiments, the charging rate, ds/dt, is prescribed, and the stress is measured as a function of time. Thus, with knowledge of the material properties of the film (ν_f, E_f, and β), the plastic strain rate in our experiments, $1/\lambda^P\, d\lambda^P/dt$, can be calculated as a function of time. Fig. 3 shows the experimental values of the terms in Eq. (7) subject to the electrochemical cycling conditions of Fig. 1. The elastic component of the strain rate is calculated using a representative value of the biaxial modulus of $E_f/(1-\nu_f) = 45$ GPa, as reported in by Sethuraman et al. [39]. In their study, they found this quantity to vary only slightly with lithium concentration over the range of concentrations examined in our studies; thus, in constructing Fig. 3, we take the biaxial modulus as a constant. The lithiation-induced strain rate is calculated using the prescribed charging rate, (ds/dt), and a value of $\beta = 2.8$, as previously discussed. The plastic component of the strain rate is then computed using Eq. (7). As can be seen from Fig. 3, during the majority of our experiments, the elastic component of the strain rate is small compared to the lithiation-induced strain rate, thereby eliminating the need to know the value of the biaxial modulus to calculate the plastic strain rate. In this limit, Eq. (7) becomes.

$$-\frac{1}{\lambda^P}\frac{\mathrm{d}\lambda^P}{\mathrm{d}t}=\frac{\beta}{3(1+\beta s)}\frac{\mathrm{d}s}{\mathrm{d}t}. \tag{8}$$

Eq. (8) has a straightforward physical interpretation: the plastic strain rate in the experiments is directly prescribed by the charging rate. By increasing the charging rate, we correspondingly impose an increased rate of plastic strain.

Combining our stress measurements with Eq. (8), we can obtain a relationship between the rate of plastic strain and the stress in the a-Li_xSi, thereby extracting material parameters. In particular, we will compare our data to a typical viscoplastic power-law [22,40]:

$$-\frac{1}{\lambda^P}\frac{\mathrm{d}\lambda^P}{\mathrm{d}t}=A\left[\frac{\sigma-\sigma_Y}{\sigma_Y}\right]^m, \tag{9}$$

where A, m, and σ_Y are fitting parameters. In this equation, σ_Y can be interpreted as the yield stress of the material at a vanishing plastic strain rate. Eq. (9) is applicable only when the stress exceeds σ_Y. In the equation, σ represents the magnitude of the measured stress (a positive quantity), and the leading negative sign is a result of the compressive stress state during lithiation. One complicating factor in our experiments is that the yield stress varies with the state of charge, as can be seen in the first cycle in Fig. 2. To mitigate this complication, we have performed the strain-rate experiment over a concentration range in which the yield stress changes slowly with lithium concentration (Fig. 2).

Upon changing the charging rate from the nominal rate of C/8 to a different rate (e.g., C/16), the stress quickly progresses toward a new value (Fig. 2b). To use these data, we rewrite Eq. (9) in a convenient form:

$$-\frac{1}{\lambda^P}\frac{\mathrm{d}\lambda^P}{\mathrm{d}t}=A\left[\frac{\left(\sigma-\sigma_{C/8}\right)+\left(\sigma_{C/8}-\sigma_Y\right)}{\sigma_{C/8}-\left(\sigma_{C/8}-\sigma_Y\right)}\right]^m, \tag{10}$$

where $\sigma_{C/8}$ represents the stress at the nominal charging rate of C/8, and all of the stresses represent the magnitude of the measured stresses (positive quantities). We assume that $(\sigma_{C/8}-\sigma_Y)$ is constant, independent of the lithium concentration over the range of concentrations considered in the experiments. After each change in the charging rate, we measure the quantity $(\sigma-\sigma_{C/8})$. We also measure the quantity $\sigma_{C/8}$ immediately before (or after) each change in the charging rate. During the experiment, the charging rate, and hence the plastic strain rate (Eq. (8)) is prescribed as a function of time. Thus, we obtain a set of data to which we can compare Eq. (10) using the quantities A, m, and $(\sigma_{C/8}-\sigma_Y)$ as fitting parameters.

Fig. 4 shows the best fit of Eq. (10) to the data from the experiment corresponding to Fig. 2. As is evident from Fig. 4, the power-law form represents the data well. The results of the best fits for three such experiments are shown in Table 1. The exponent m, has values in the range of 2.58–4.07. For large values of m, the stress level is insensitive to the applied strain rate and is instead limited by the yield strength, σ_Y. In our experiments, the measured values of m demonstrate a moderate level of strain-rate sensitivity.

As a final note, this experimental technique could be used to measure rate-sensitive material properties as a function of lithium concentration by repeating the outlined procedure at various states of charge. In our experiments, we subject the film to the same set of (nominal) charging rates twice (Fig. 2b). There is little variation in the extracted material parameters from each set of charging rates. It is of course possible that these properties could vary with the state of charge if we were to study a larger range of lithium concentrations; such work was not pursued in this paper.

4. Discussion

Our results indicate that a-Li_xSi electrodes are rate sensitive at room temperature and that the rate effect is important at charging rates typically used in lithium-ion batteries. These observations have significant ramifications for the rate-capabilities of silicon anodes. In particular, due to the strain-rate sensitivity, faster charging will result in larger stresses, which may result in fracture of the electrode.

We should first mention that a recent work by Boles et al. has investigated creep deformation in lithiated silicon [41]. In their work, constant-force creep tests were conducted on fully lithiated c-$Li_{15}Si_4$ nanowires. Their investigation was primarily performed at stress levels below the apparent yield stress of the material. Interestingly, at these low stress levels, the authors found a linear relationship between the strain rate and the stress, suggesting Newtonian viscous flow of c-$Li_{15}Si_4$ [41]. The nanowires tested by Boles et al. are polycrystalline; thus, the grain boundaries may

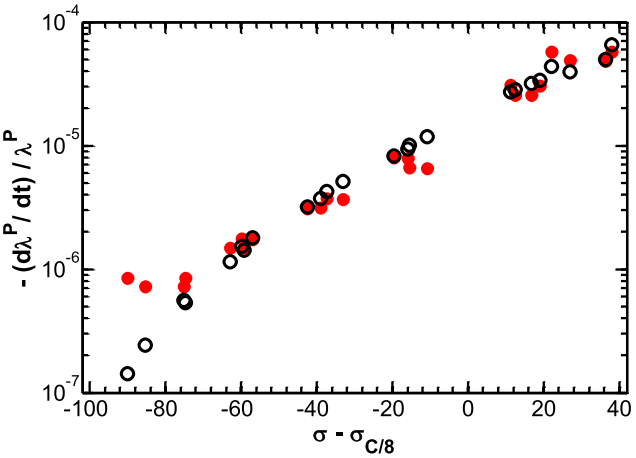

Fig. 4. Plastic strain rate (in units of s^{-1}) versus the change in measured stress relative to the C/8 rate (in units of MPa). The solid red circles represent the experimental data and the open black circles represent the phenomenological model presented in Eq. (10). (For interpretation of the references to colour in this figure legend, the reader is referred to the web version of this article.)

Table 1
Results of the fit of the experimental data to the phenomenological model, Eq. (10), for three separate experiments.

A (1/s)	m	$\sigma_{C/8} - \sigma_Y$ (MPa)	R^2
0.00175	4.07	130	0.947
0.00230	2.94	94.1	0.937
0.00168	2.58	82.9	0.892

allow diffusional transport as well as creep deformation [41]. Moreover, their testing of the crystalline phase allows for the possibility of creep deformation via dislocation motion. In the present work, we focus on quantifying the relationship between the charging rate and the resulting stresses during electrochemical cycling of a-Li_xSi. We use charging rates typical of lithium-ion batteries and examine a range of lithium concentrations. We also limit the depth of discharge in this study to investigate amorphous electrodes, which are typically used in practice due to their improved cycling performance [42]. Since the material is amorphous, there are no dislocations. Even so, we observe a significant rate effect. Due to the large strains associated with lithiation/delithiation, stresses in Li_xSi electrodes readily reach the yield stress during cycling. At these large stresses, different from Boles et al., we observe a non-linear relationship between the stress and the strain rate. Our results can answer a number of open questions in literature, as will now be discussed.

Our observations of rate-sensitive plasticity in a-Li_xSi shed light on recent theories and experiments. For instance, Soni et al. found fracture only at large charging rates ($\geq C/2$) in 150 nm silicon thin films [33]. The authors attributed this observation to diffusion limitations through the thickness of the film [33]. It is also possible that their observations are due to effects of rate-sensitive plasticity: for the range of charging rates used in our experiments (C/128 to C/2), the stresses varied by over 100 MPa. These variations in stress will significantly alter the driving force for fracture, as the energy release rate scales with the square of the stress. Thus, substantially larger crack-driving forces develop at larger charging rates, potentially leading to fracture.

As another example, Brassart and Suo have suggested that inelasticity in batteries may occur by two processes: flow and reaction [30]. "Flow" changes the shape of the electrode while preserving volume and lithium concentration, and is driven by the deviatoric stress — a process similar to plastic flow in a metal. By contrast, "reaction" (i.e., lithium insertion/removal) changes both volume and lithium concentration. "Reaction" is driven by a combination of the mean stress and the chemical potential of lithium in the environment [30]. These two processes, flow and reaction, are intimately coupled as they both involve the same physical processes: breaking and forming atomic bonds. As a result of this chemo-mechanical coupling, larger overpotentials (i.e., larger chemical driving forces) can result in flow at a smaller stress [30]. In our experiments, larger charging rates result in larger overpotentials. Thus, in the absence of any other rate effects, Brassart and Suo would predict a decrease in the magnitude of the flow stress with increasing charging rate. In contrast, we see the opposite trend in our experiments – larger charging rates result in an increase in the magnitude of the flow stress. Therefore, as previously discussed, we believe that our results are indicative of a material rate effect: a-Li_xSi is strain-rate sensitive. Larger charging rates result in larger strain rates in the material, which in turn generate larger stresses. We should note, however, that our experiments do not preclude the existence of the so-called "reactive flow" effects discussed by Brassart and Suo. It is possible that these effects do indeed exist, but that they are too small relative to the strain-rate dependence of the material to be observed in our experiments. For instance, our results are qualitatively consistent with a model of Brassart and Suo that incorporates both "reactive flow" effects and material rate-effects [29].

Additionally, Pharr et al. have suggested that a-Li_xSi demonstrates a peculiar ability to both flow plastically and fracture in a brittle manner [5]. The authors did not speculate as to the physics governing this curious combination of properties. However, when a crack propagates in a-Li_xSi, it moves relatively fast, resulting in large strain-rates near the crack tip. In this paper, we provide evidence for rate-sensitivity of a-Li_xSi: plastic flow at larger strain-rates requires larger stresses. Consequently the strains associated with fracture are mostly elastic, and the material fails in a brittle fashion, in agreement with fractographic observations and justifying the use of linear elastic fracture mechanics as employed in Ref. [5].

The discussion herein underscores the importance of determining the exact microscopic picture governing plastic flow in a-Li_xSi. Some potential mechanisms have been investigated through computational atomistic simulations. For instance, Zhao, et al. found that continuous bond breaking and re-forming assisted by Li insertion can accommodate large plastic deformation [24]. In another study, Zhao, et al. found bond switching to occur at loosely packed free-volume regions, leading to localized plastic deformation [34]. Such deformation is reminiscent of that found in metallic glasses. It has been established that an applied stress can cause local atomic rearrangement in metallic glasses, resulting in macroscopic deformation. In particular, a flow equation is usually implemented from transition-state theory, in which the strain-rate scales with the stress as $\dot{\varepsilon} \propto \sinh(\tilde{\Omega}\sigma/2kT)$, where $\tilde{\Omega}$ is the activation volume, k is the Boltzmann constant, and T is the temperature [43–45]. Over a particular range of stress, this scaling is quite similar to that of Eq. (9), which was found to describe our data well (Table 1). Although this similarity does not definitively point to a particular microscopic mechanism, it suggests that deformation of a-Li_xSi shares some of the same features as metallic glasses. In another atomistic study, Huang and Zhu attributed plastic deformation during lithiation of silicon to a decrease in strong covalent Si–Si bonds and an increase in weak Li–Li bonds [26]. The high mobility of Li atoms facilitates effective bond switching to accommodate mechanical deformation [26]. Thus, it further appears that bond breaking and re-forming, as well as the mobility of lithium are important for plastic deformation of a-Li_xSi. These processes take time and thus engender rate-dependent plasticity. Unfortunately, due to computational limitations of atomistic simulations, the time scales associated with these processes are not well understood. Our current work emphasizes the importance of gaining a better understanding the dynamics of plastic flow in a-Li_xSi, and thus warrants future theoretical and computational studies.

5. Conclusions

We have measured stresses in silicon thin films as a function of the charging rate. Increasing the rate of lithiation resulted in a corresponding increase in the flow stress. Our results indicate that rate-sensitive plasticity occurs in a-Li_xSi at room temperature and at charging rates typically used in lithium-ion batteries. To extract material parameters, we have developed a model of concurrent lithiation and rate-sensitive plasticity. The data are well described by a power-law relationship between the strain-rate and the stress, with a value of the stress exponent, m, in the range of 2.58–4.07, indicating a moderate level of strain-rate sensitivity. These results provide insight into the unusual ability of a-Li_xSi to flow plastically but fracture in a brittle manner. Moreover, the results have direct ramifications concerning the rate-capabilities of silicon anodes. In particular, faster charging rates result in larger stresses, which can lead to fracture of the electrode. We hope that this work will

provide guidance for the design of future theoretical models that account for material rate effects. Likewise, we hope that this work will inspire future computational studies aimed at understanding the dynamics of plastic flow in a-Li_xSi.

Acknowledgments

We thank Frans Spaepen for a number of useful discussions pertaining to this work. This work was supported by the National Science Foundation through a grant on Lithium-ion Batteries (CMMI-1031161). It was performed in part at the Center for Nanoscale Systems, a member of the National Nanotechnology Infrastructure Network, which is supported by the National Science Foundation under NSF Award No. ECS-0335765, and at the Harvard University Materials Research Science and Engineering Center, which is supported by the National Science Foundation under Award No. DMR-0820484. M.P. acknowledges support by the National Science Foundation Graduate Research Fellowship Program.

Appendix A. Experimental procedure

Cover glass substrates with a thickness of 175 μm were cleaned with acetone and isopropanol and placed into a sputter deposition system (AJA Int. ATC 1800) with a base pressure of $<10^{-8}$ Torr. All sputtering targets have a 50.8 mm diameter, and depositions were performed at room temperature (22 °C). The samples were plasma-cleaned in Ar at 20 mTorr and an RF power of 24 W for 5 min. Next, 15 nm of Ti was sputtered onto the substrates using a pressure of 3 mTorr of Ar and a DC power of 100 W for 5 min. A 300 nm layer of Cu was then deposited on the Ti underlayer using a pressure of 5 mTorr of Ar and a DC power of 100 W for 15 min. The Cu film serves as current collector, while the Ti underlayer is used to improve the adhesion between the Cu film and the glass substrate. Finally, a 100 nm Si film was deposited on the Cu current collector using a pressure of 5 mTorr of Ar and a DC power of 100 W for 27 min. The thickness of the film was verified using profilometry, and was found to be 100 ± 10 nm. The working area of each silicon electrode is 8 mm by 30 mm. We have previously performed X-ray diffraction experiments to confirm that the silicon films are amorphous under these sputtering conditions [27].

Electrochemical experiments were conducted in a custom-fabricated hermetic Teflon electrochemical cell with a glass window. The cell was assembled in a three-electrode configuration in an argon-filled glovebox, which was maintained at <1 ppm moisture. The sputtered silicon film was used as the working electrode, and Li foil was used as the reference electrode and the counter electrode. A 1 M solution of $LiPF_6$ in 4:3:3 (vol %) ethylene carbonate : dimethyl carbonate : diethyl carbonate with a vinylene carbonate additive was used as the electrolyte (MTI Corporation). Electrochemical measurements were performed with a VersaSTAT 3 galvanostat from Princeton Applied Research. During the first cycle, the cell was tested galvanostatically at a current density of 23.6 μA cm^{-2} (a C/8 rate assuming a capacity of 3579 mAh g^{-1} [36]) between 0.8 and 0.05 V vs. Li/Li^+. The lower cutoff potential of 50 mV vs Li/Li^+ was employed to prevent crystallization of the a-Li_xSi electrodes [42]. Relatively thin films (100 nm) and an upper cutoff potential of 0.8 V vs Li/Li^+ were employed to prevent fracture during delithiation. During the second cycle, the cell was lithiated at a C/8 rate for 1 h, followed by a number of segments with different charging rates. The duration of these segments was fixed such that the total capacity during each segment was 50 mAh g^{-1} (1.4% of the total capacity of 3579 mAh g^{-1}). The relatively slow charging rates used in these experiments were selected to allow enough time for diffusive equilibrium through the films [11,46,47]. We use the data measured during the second cycle to minimize effects of SEI growth [11].

The stress in the film was measured by monitoring the curvature of the substrate in-situ during electrochemical testing. The average stress in the film was deduced from the curvature via Stoney's equation [48,49]:

$$\sigma = \sigma_r + \frac{E_s h_s^2}{6 h_f (1-\nu_s)} \Delta K, \tag{11}$$

where σ is the average stress in the film, E_s is the elastic modulus of the substrate, h_s is the thickness of the substrate, h_f is the thickness of the film, ν_s is Poisson's ratio of the substrate, and ΔK is the change in the curvature of the substrate that results from the stress in the film. σ_r is the residual stress in the film that develops during sputter deposition and is determined from substrate curvature measurements before and after deposition of the film. In our calculations, we have used values of $E_s = 77$ GPa and $\nu_s = 0.22$ for the glass substrates. We should also note that in a previous study, we have determined that the stresses measured in our experiments result almost entirely from lithiation of the silicon film as opposed to SEI growth [5]. Nadimpalli et al. have found a similar result for 100 nm Si films [50]. As a result, we have neglected any contribution of the SEI to the measured stress.

From Eq. (11), it is clear that knowledge of properties of the film other than film thickness is not required to evaluate the stress. As in our previous work [5], we take the thickness of the film, h_f, to depend linearly on the state of charge:

$$h_f = h_f^0 (1 + \beta s), \tag{12}$$

where h_f^0 is the initial film thickness, β is related to the atomic volumes (Ω) by $\beta = (\Omega_{Li_{15}Si_4} - \Omega_{Si})/\Omega_{Si}$, and s is the state of charge, with a value of 0 representing pure silicon and a value of 1 representing the fully lithiated state (assumed to be a-$Li_{15}Si_4$ with a capacity of 3579 mAh g^{-1}) [36]. Obrovac et al. found a 280% increase in the volume of silicon upon reaching the fully lithiated state of $Li_{15}Si_4$ [36], i.e., $\beta = 2.8$.

The curvature of the substrate was monitored with a multi-beam optical sensor (MOS) from k-Space Associates. The MOS employs an array of parallel laser beams to measure the curvature of the substrate. The array of laser beams allows simultaneous illumination and detection, which in turn greatly reduces noise in the measurements caused by fluid motion in the electrochemical cell or by ambient vibrations. The cell was also placed on an anti-vibration table during testing. The change in the curvature of the substrate was calculated from the geometric relation.

$$\Delta K = \frac{d_0 - d}{d_0} \left[\frac{\cos\alpha}{2L}\right] \frac{n_a}{n_e}, \tag{13}$$

where d is the distance between two adjacent laser spots measured on the CCD camera, d_0 is the initial distance between the laser spots, α is the angle of reflection of the laser beams, L is the distance between the electrochemical cell and the CCD camera, and n_a and n_e are the indices of refraction of air and the electrolyte, respectively. Since the laser beams pass through air, the electrolyte, and an optical window, refraction of the beams at these corresponding interfaces must be taken into account, which is the source of the quantity n_a/n_e. In the calculation of the stress, we have taken $n_e = 1.42$ for the electrolyte [51] and $n_a = 1$ for air. A combination of Eqs. (11)–(13) allows for calculation of the average stress in the a-Li_xSi films during electrochemical testing. A more detailed explanation of this technique is provided in Ref. [5]

References

[1] W.J. Zhang, J. Power Sources 196 (2011) 13–24.
[2] L.Y. Beaulieu, K.W. Eberman, R.L. Turner, L.J. Krause, J.R. Dahn, Electrochem. Solid State Lett. 4 (2001) A137–A140.
[3] R. Deshpande, M. Verbrugge, Y.T. Cheng, J. Wang, P. Liu, J. Electrochem. Soc. 159 (2012) A1730–A1738.
[4] S.P.V. Nadimpalli, V.A. Sethuraman, S. Dalavi, B. Lucht, M.J. Chon, V.B. Shenoy, P.R. Guduru, J. Power Sources 215 (2012) 145–151.
[5] M. Pharr, Z. Suo, J.J. Vlassak, Nano Lett. 13 (2013) 5570–5577.
[6] C.K. Chan, H. Peng, G. Liu, K. Mcllwrath, X.F. Zhang, R.A. Huggins, Y. Cui, Nat. Nanotech 3 (2008) 31–35.
[7] K. Peng, J. Jie, W. Zhang, S.-T. Lee, Appl. Phys. Lett. 93 (2008) 033105.
[8] T. Takamura, S. Ohara, M. Uehara, J. Suzuki, K. Sekine, J. Power Sources 129 (2004) 96–100.
[9] H. Haftbaradaran, X. Xiao, M.W. Verbrugge, H. Gao, J. Power Sources 206 (2012) 357–366.
[10] C. Yu, X. Li, T. Ma, J. Rong, R. Zhang, J. Shaffer, Y. An, Q. Liu, B. Wei, H. Jiang, Adv. Energy Mater. 2 (2012) 68–73.
[11] S.K. Soni, B.W. Sheldon, X. Xiao, A. Tokranov, Scr. Mater. 64 (2011) 307–310.
[12] S.K. Soni, B.W. Sheldon, X. Xiao, M.W. Verbrugge, D. Ahn, H. Haftbaradaran, H. Gao, J. Electrochem. Soc. 159 (2012) A38–A43.
[13] L. Baggetto, D. Danilov, P.H.L. Notten, Adv. Mater. 23 (2011) 1563–1566.
[14] H. Zhang, P.V. Braun, Nano Lett. 12 (2012) 2778–2783.
[15] Y. Yao, M.T. McDowell, I. Ryu, H. Wu, N. Liu, L. Hu, W.D. Nix, Y. Cui, Nano Lett. 11 (2011) 2949–2954.
[16] H. Wu, G. Chan, J.W. Choi, I. Ryu, Y. Yao, M.T. McDowell, S.W. Lee, A. Jackson, Y. Yang, L. Hu, Y. Cui, Nat. Nanotechnol. 7 (2012) 309–314.
[17] B. Hertzberg, A. Alexeev, G. Yushin, J. Am. Chem. Soc. 132 (2010) 8548–8549.
[18] V.A. Sethuraman, M.J. Chon, M. Shimshak, V. Srinivasan, P.R. Guduru, J. Power Sources 195 (2010) 5062–5066.
[19] J.Y. Huang, L. Zhong, C.M. Wang, J.P. Sullivan, W. Xu, L.Q. Zhang, S.X. Mao, N.S. Hudak, X.H. Liu, A. Subramanian, H. Fan, L. Qi, A. Kushima, J. Li, Science 330 (2010) 1515–1520.
[20] K. Zhao, M. Pharr, J.J. Vlassak, Z. Suo, J. Appl. Phys. 109 (2011) 016110.
[21] K. Zhao, M. Pharr, S. Cai, J.J. Vlassak, Z. Suo, J. Am. Ceram. Soc. 94 (2011) S226–S235.
[22] A.F. Bower, P.R. Guduru, V.A. Sethuraman, J. Mech. Phys. Solids 59 (2011) 804–828.
[23] B. Hertzberg, J. Benson, G. Yushin, Electrochem. Commun. 13 (2011) 818–821.
[24] K. Zhao, W.L. Wang, J. Gregoire, M. Pharr, Z. Suo, J.J. Vlassak, E. Kaxiras, Nano Lett. 11 (2011) 2962–2967.
[25] F. Fan, S. Huang, H. Yang, M. Raju, D. Datta, V.B. Shenoy, A.C.T. van Duin, S. Zhang, T. Zhu, Modell. Simul. Mater. Sci. Eng. 21 (2013) 074002.
[26] S. Huang, T. Zhu, J. Power Sources 196 (2011) 3664–3668.
[27] K. Zhao, G.A. Tritsaris, M. Pharr, W.L. Wang, O. Okeke, Z. Suo, J.J. Vlassak, E. Kaxiras, Nano Lett. 12 (2012) 4397–4403.
[28] K. Zhao, M. Pharr, Q. Wan, W.L. Wang, E. Kaxiras, J.J. Vlassak, Z. Suo, J. Electrochem. Soc. 159 (2012) A238–A243.
[29] L. Brassart, Z. Suo, Int. J. Appl. Mech. 4 (2012) 1250023.
[30] L. Brassart, Z. Suo, J. Mech. Phys. Solids 61 (2013) 61–77.
[31] Z. Cui, F. Gao, Z. Cui, J. Qu, J. Power Sources 207 (2012) 150–159.
[32] B.W. Sheldon, S.K. Soni, X. Xiao, Y. Qi, Electrochem. Solid State Lett. 15 (2012) A9–A11.
[33] S.K. Soni, B.W. Sheldon, X. Xiao, A.F. Bower, M.W. Verbrugge, J. Electrochem. Soc. 159 (2012) A1520–A1527.
[34] K. Zhao, Y.G. Li, L. Brassart, Acta Mech. Sin. 29 (2013) 379–387.
[35] G. Bucci, S.P.V. Nadimpalli, V.A. Sethuraman, A.F. Bower, P.R. Guduru, J. Mech. Phys. Solids 62 (2014) 276–294.
[36] M.N. Obrovac, L.J. Krause, J. Electrochem. Soc. 154 (2007) A103–A108.
[37] Y. He, X. Yu, G. Li, R. Wang, H. Li, Y. Wang, H. Gao, X. Huang, J. Power Sources 216 (2012) 131–138.
[38] L.Y. Beaulieu, T.D. Hatchard, A. Bonakdarpour, M.D. Fleischauer, J.R. Dahn, J. Electrochem. Soc. 150 (2003) A1457–A1464.
[39] V.A. Sethuraman, M.J. Chon, M. Shimshak, N. Van Winkle, P.R. Guduru, Electrochem. Commun. 12 (2010) 1614–1617.
[40] J.L. Chaboche, Int. J. Plast. 5 (1989) 247–302.
[41] S.T. Boles, C.V. Thompson, O. Kraft, R. Moenig, Appl. Phys. Lett. 103 (2013) 263906.
[42] M.N. Obrovac, L. Christensen, Electrochem. Solid State Lett. 7 (2004) A93–A96.
[43] F. Spaepen, Acta Metall. 25 (1977) 407–415.
[44] M. Heggen, F. Spaepen, M. Feuerbacher, J. Appl. Phys. 97 (2005) 033506.
[45] T. Egami, T. Iwashita, W. Dmowski, Metals 3 (2013) 77–113.
[46] M. Pharr, K. Zhao, X. Wang, Z. Suo, J.J. Vlassak, Nano Lett. 12 (2012) 5039–5047.
[47] V.B. Shenoy, P. Johari, Y. Qi, J. Power Sources 195 (2010) 6825–6830.
[48] G.G. Stoney, Proc. R. Soc. Lond. Ser. A 82 (1909) 172–175.
[49] W.D. Nix, Metall. Trans. A 20 (1989) 2217–2245.
[50] S.P.V. Nadimpalli, V.A. Sethuraman, G. Bucci, V. Srinivasan, A.F. Bower, P.R. Guduru, J. Electrochem. Soc. 160 (2013) A1885–A1893.
[51] M.A. McArthur, S. Trussler, J.R. Dahn, J. Electrochem. Soc. 159 (2012) A198–A207.